J Eng Math (2009) 64:353–365
DOI 10.1007/s10665-009-9285-z

Flow in a multi-branching vessel with compliant walls

J. E. F. Green · F. T. Smith · N. C. Ovenden

Received: 1 May 2008 / Accepted: 2 March 2009 / Published online: 28 March 2009

Abstract The problem of fluid flow in a compliant-walled channel which branches into two or more daughters is considered with the aim of understanding blood flow through arterio-venous malformations (AVMs) in the brain. The outer walls of the channel are assumed for definiteness to behave as spring-back plates, whilst the divider is taken as rigid. The fluid is assumed to be incompressible and inviscid. When the Strouhal number is small (as occurs in practice in the brain), there are two main axial length scales, one much longer than the vessel width and the other comparable with the vessel width. Also, in the case of small wall displacements, one can analyse the local flow-structure interaction problem using a complex variable method. The flow shows markedly different qualitative features downstream of the branching, depending on the wall stiffness.

Keywords Branching channel · Compliant walls · Inviscid fluid flow · Matching

1 Introduction

This study, like those of [1–5], is motivated by a desire to improve our understanding of the blood flow through arterio-venous malformations (AVMs) in the brain. In an AVM, an artery branches abruptly into numerous (perhaps ~ 20) smaller vessels, which in turn drain into the venous system. (In practice, an AVM may have several feeding arteries and draining veins attached to it; however, here we shall, for the sake of simplicity, focus on the case of a single feeding artery.) The prevalence of AVMs is approximately 1 in 1000 people, and they represent a difficult clinical problem, being associated with increased risk of haemorrhage (including potentially fatal stroke) and epilepsy. These risks arise because the AVM structure often appears to offer a comparatively small overall vascular

J. E. F. Green (✉) · F. T. Smith · N. C. Ovenden
Department of Mathematics, University College London, Gower Street, London WC1E 6BT, UK
e-mail: egreen@mbi.osu.edu

J. E. F. Green
Mathematical Biosciences Institute, The Ohio State University, Columbus, OH 43210, USA

F. T. Smith
e-mail: frank@math.ucl.ac.uk

N. C. Ovenden
e-mail: nicko@math.ucl.ac.uk

resistance, resulting in a considerably greater rate of blood flow than is typically observed between the arterial and venous systems. This, in turn, leads to 'steal' phenomena, where large flow rates through the AVM reduce cerebral throughput elsewhere. Surgical interventions used to reduce the flow rate through the AVM are largely empirically based, and include clipping and glue casting.

There are thus several questions which modelling studies might seek to address. Firstly, what is the flow through the AVM, and how or when does it give rise to such high flow rates? Secondly, what is the effect of the presence of an AVM within a network of blood vessels, such as the cranial network? Thirdly, why (and under what conditions) are the currently used surgical procedures effective at reducing the flow rate? In fact, a number of studies have been undertaken (or are in progress) to try to answer each of these questions [4,6], but we concentrate on the first one here.

Flows in branching channels and tubes have been of longstanding interest, many motivated by the finding that fatty streaks (which can lead to atherosclerosis) preferentially accumulate in the outer walls of dividing arteries. This accumulation is thought to be correlated with low wall shear stress [7]. The bifurcating channel problem for steady high Reynolds number (Re) flow was analysed by Smith [8], who used boundary-layer theory to determine the flow on $O(Re)$ lengthscales for small turning angles. His paper also addressed the similar three-dimensional problem in which a cylindrical tube is split into two tubes of semicircular cross section by the insertion of a flat plate. This problem was revisited by Blyth and Mestel [9], who considered the flow over $O(1)$ lengthscales, and extended by Tadjfar and Smith [5] to the case of non-zero branching angles using a combination of direct numerical simulations, and analysis for the case of slender tubes. A similar problem, where there is a side branch (small daughter) off a main tube, was considered in [3]; a notable feature in that case is the large pressure jump close to the mouth of the side branch.

Branching-tube and channel flows where there are more than two daughters (the case more applicable to AVMs) were considered in [1]. In this study, the dividers are taken to be of thickness $O(Re^{-\frac{1}{3}})$ (with $Re \gg 1$); the perturbation to the incident velocity profile is assumed to be of the same order, resulting in a linear system of equations. One of the main results of this paper was that the core flow is affected most by the middle divider shapes, and little by the outer walls. In a later paper [2], the authors neglect viscous effects, but relax the assumption that the perturbation to the oncoming flow is small. They consider a two-dimensional geometry in which their model can be reduced to a system of nonlinear recurrence relations which are solved numerically, and analytically in the limit of a large number of daughters. An interesting feature of this work is that non-unique solutions for the outflows from the daughter channels are found. Of perhaps greater clinical relevance is the fact that the total mass flux increases almost linearly with the number of daughters, even though the total downstream flow area remains fixed. The related problem, of flow through a network of successive bifurcations was considered in [6]. Increasing the imposed pressure drop, or vessel cross-sections, in one half of the network (with those in the other half being held fixed) was found to result in an increased overall flux.

Fluid flows through compliant-walled vessels are of course ubiquitous throughout the human body, with the vascular and pulmonary systems being a particular focus of theoretical studies. A popular and simple device for investigating so-called fluid-structure interactions is known as the Starling Resistor. It comprises two lengths of rigid tubing, connected by a thin walled elastic tube subject to external compression. Fluid is driven through the device by an imposed pressure drop, and typical Reynolds numbers are in the range 10^2–10^4 [10]. The behaviour of this system has been the subject of a number of theoretical investigations [11–13], whilst other studies have considered channels or tubes which have compliant walls along their entire length [14–17]. The theoretical problem in full is extremely complex, and it is very difficult to make any progress analytically. The earliest one-dimensional models, whilst being reasonably tractable and providing useful insights into phenomena such as choking, and self-excited oscillations, involve some ad hoc assumptions, and as a result do not appear to give good quantitative agreement with experiments [10]. More recent work has examined rational approximations of two- or three-dimensional models for high Reynolds number flows; some additional assumptions are usually required to make the model tractable, such as small wall displacement (or small disturbance to the base flow) [11,12,14,17], prescribed wall motion [16] or high wall oscillation frequency [12,16]. In all of these cases, there is only one channel (or tube), the centreline of which is straight.

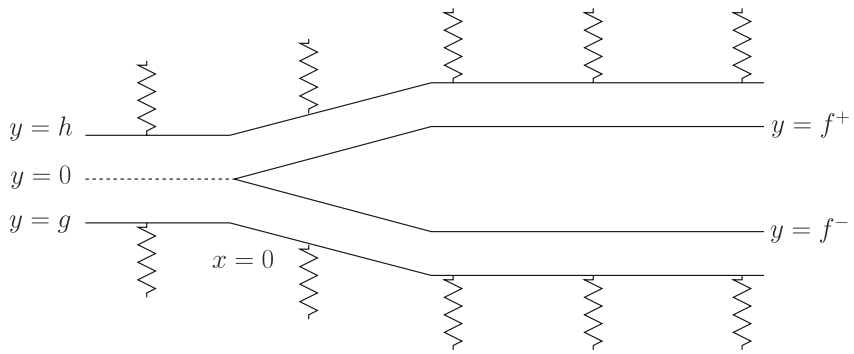

Fig. 1 Definition sketch

Here, we seek to extend earlier work on AVMs in which the channel walls were assumed to be rigid by considering the effect of introducing compliant walls. This in turn extends previous studies of compliant-walled channel flows which have considered single non-branching tubes or channels. Another extension is involved in the interesting feature that the theory here can accommodate non-small displacements of the compliant walls. However, our model does contain a number of idealisations (such as the neglect of viscous effects, and use of a simplified wall model) which mean we are not yet in a position to make quantitative comparisons with experimental or clinical observations. It is a first step, which we hope will help to point the way for future studies.

This paper is organised as follows. Our simplified model is formulated in Sect. 2 as a system of coupled partial differential equations describing the fluid flow and wall motion. We begin in Sect. 3 by considering the flow over long lengthscales. We find that wave behaviour applies, similar to that described classically for a single long vessel; however, the pressure and velocity may jump at any branch point. In Sect. 4, we consider the flow close to the branching point for small Strouhal number. In the simple case of irrotational flow with small wall displacements, we are able to use a complex variable method to gain insight into the behaviour of the solution. We conclude in Sect. 5 with a summary of our main findings and suggestions for future research.

2 Model formulation

We consider a two-dimensional channel which branches into two daughters, as shown in Fig. 1. The case of more daughters will be discussed in Sect. 5. As in [2], the blood is assumed incompressible and inviscid, and the flow has velocity components u and v in the x- and y-directions, respectively. Far upstream of the branching, the mother channel is straight, and we take the centreline to be $y = 0$. In the region $x > 0$, there is a rigid divider which splits the flow into two daughter channels. The upper and lower surfaces of the divider are given by $y = f^+(x)$ and $y = f^-(x)$, respectively. The compliant upper and lower walls of the channel are located at $y = h$ and $y = g$, respectively. Where necessary, quantities associated with the mother are identified by the superscript m, and those associated with the upper and lower daughter channels by the superscripts + and − respectively.

The fluid flow is governed by the continuity and Euler equations:

$$u_x + v_y = 0, \tag{2.1}$$

$$u_t + uu_x + vu_y = -\frac{p_x}{\rho}, \quad v_t + uv_x + vv_y = -\frac{p_y}{\rho}, \tag{2.2}$$

where ρ is the density of the blood. The flow is subject to the usual kinematic boundary conditions on the compliant walls $y = g, h$

$$v|_{y=g} = g_t + ug_x, \quad v|_{y=h} = h_t + uh_x, \tag{2.3}$$

and no penetration conditions on the divider walls $y = f^{\pm}(x)$

$$v = uf_x^{\pm} \quad \text{on } y = f^{\pm}. \tag{2.4}$$

The compliant walls of the vessels are modelled as spring-backed plates which are constrained to move only in the y-direction. Although this is a gross simplification of the true behaviour of the arterial wall (see e.g. [18] for a review of artery wall models), it has the obvious advantage of rendering the resulting problem more tractable as a first step. Similar models have previously been used in [19,20] in connection with the study of airway reopening problems in the lungs. Furthermore, measurements of the vessel diameter and pressure waveform for the canine aorta, reproduced in [21], appear to support our assumption of a linear pressure-channel width relation, at least as an initial approximation. A more complicated wall model (valid for small wall displacements) was presented in [14], which included non-zero wall damping coefficient, flexural rigidity and longitudinal tension, all of which are assumed to be zero here. We note the results of [15] suggest that neglect of these parameters may lead to very different behaviour to that which is observed when they are non-zero, and thus our simplified wall model might need to be approached with caution.

Taking the equilibrium wall positions to be $y = g^*, h^*$, we then set $g = g^* + \eta^-$, $h = h^* + \eta^+$, where $\eta^\pm$ are the wall displacements. These then obey

$$M\eta^-_{tt} = p|_{y=g} n_y - \kappa\eta^-, \quad M\eta^+_{tt} = p|_{y=h} n_y - \kappa\eta^+, \tag{2.5}$$

where n_y is the y-component of the unit outward normal to the wall, M is the mass per unit length, and κ is the spring constant, which are assumed to be the same for both walls.

In general, we specify the pressure P_{in} far upstream of the branching in the mother, and at some point far downstream in the daughters, as in [2]. The pressures far downstream of the branching are thus P^+_∞, P^-_∞. However, we shall also consider the situation where the fluxes are specified. At the branching point, we require three conditions, which are continuity of momentum flux between the mother and each daughter (for irrotational flow, this reduces to continuity of the quantity $p + \frac{1}{2}|\boldsymbol{u}|^2$, as in [22]) and overall conservation of mass flux

$$Q^m(0, y, t) = Q^+(0, y, t) + Q^-(0, y, t). \tag{2.6}$$

2.1 Nondimensionalisation

We take h_{in} and U_{in} to be the values of h and u far upstream of the branching ($x \to -\infty$), and let T be the timescale of pressure variations due to the cardiac cycle. We then nondimensionalise the governing equations as follows (where tildes indicate dimensionless quantities)

$$t = T\tilde{t}, \quad (x, y, g, h, f^\pm) = h_{\text{in}}(\tilde{x}, \tilde{y}, \tilde{g}, \tilde{h}, \tilde{f^\pm}), \quad (u, v) = U_{\text{in}}(\tilde{u}, \tilde{v}), \quad p = \rho U^2_{\text{in}}\tilde{p}, \quad Q = U_{\text{in}}h_{\text{in}}\tilde{Q}.$$

The dimensionless equations are then (dropping the tildes):

$$u_x + v_y = 0, \tag{2.7}$$

$$\mathcal{S}u_t + uu_x + vu_y = -p_x, \quad \mathcal{S}v_t + uv_x + vv_y = -p_y, \tag{2.8}$$

where $\mathcal{S} = h_{\text{in}}/TU_{\text{in}}$ is the Strouhal number (ratio of flow timescale to oscillation timescale). The mean velocity of blood in the middle cerebral artery in the brain was measured as around 60–80 cm s^{-1} in [23]; maximum velocities of the order of 1 ms^{-1} are reported in [24]. Taking a typical timescale for oscillations as 1 s (based on typical adult heart rates of 60–100 beats per minute), and an arterial diameter of 0.1–0.5 cm [2] then gives $\mathcal{S} \sim O(10^{-2}–10^{-3})$.

The positions of the upper and lower walls are determined from:

$$\mu\eta^+_{tt} = pn_y - \frac{1}{k}\eta^+ \quad \text{on } y = h, \quad \mu\eta^-_{tt} = pn_y - \frac{1}{k}\eta^- \quad \text{on } y = g, \tag{2.9}$$

where $\mu = Mh_{\text{in}}/\rho U^2_{\text{in}}T^2$ is the ratio of wall inertia to fluid inertia and $k = \frac{\rho U^2_{\text{in}}}{\kappa h_{\text{in}}}$ is the ratio of fluid inertia to wall elasticity.

The kinematic boundary conditions at $y = g, h$ and no-penetration conditions on $y = f^\pm(x)$ now become

$$v = \mathcal{S}g_t + ug_x \quad \text{on } y = g, \quad v = \mathcal{S}h_t + uh_x \quad \text{on } y = h, \tag{2.10}$$

$$v = uf^\pm_x \quad \text{on } y = f^\pm. \tag{2.11}$$

Our task is therefore to understand the system (2.7–2.11) for small $\mathcal{S}$ values.

3 The flow over longer lengthscales for small Strouhal number

In the following section we shall assume $\mathcal{S} \ll 1$, as suggested by the parameter values above. We consider the behaviour of the flow over a longer horizontal lengthscale. We hence introduce the scaled coordinate, X, where

$$x = \mathcal{S}^{-1}X.$$

The solution is then assumed to take the following form in the mother and each of the daughters

$$p = P(\text{const}) + \mathcal{S}p'(X, y, t) + \cdots, \quad u = U(y) + \mathcal{S}u'(X, y, t) + \cdots,$$
$$v = \mathcal{S}^2 v'(X, y, t) + \cdots, \quad \eta = \eta_0(\text{const}) + \mathcal{S}\eta'(X, y, t) + \cdots,$$

(note we have omitted the superscripts for notational convenience). Matching is important at this stage. The leading order velocities, $U(y)$, and pressures, P, in the mother and each daughter have to be taken to be known (in fact, they are determined on the $O(1)$ lengthscale which we consider in Sect. 4). For the sake of simplicity, we will incorporate η_0 into h^*, g^*. (This implies that h^*, g^* may be discontinuous at $X = 0$, due to the $O(1)$ pressure jump on the short scale.)

On neglecting wall inertia ($\mu = 0$), the governing equations at $O(\mathcal{S}^2)$ are:

$$u'_X + v'_y = 0, \tag{3.1}$$
$$u'_t + Uu'_X + v'U_y = -p'_X, \quad p'_y = 0, \tag{3.2}$$
$$p' - \frac{1}{k}\eta'^{+} = 0 \quad \text{on } y = h^*, \quad -p' - \frac{1}{k}\eta'^{-} = 0 \quad \text{on } y = g^*. \tag{3.3}$$

At leading order the kinematic boundary conditions imply that the walls of the mother and daughter tubes must be horizontal on the long scale (i.e., $f_X = g^*_X = h^*_X = 0$) which we shall see is consistent with the short-lengthscale solution of Sect. 4.1 (provided pressure, rather than flux conditions are imposed). Continuity of momentum flux gives [4]:

$$p' + Uu' \text{ is continuous across } X = 0. \tag{3.4}$$

At next order, the kinematic boundary conditions give

$$v' = \eta'^{-}_t + U\eta^{-}_X \quad \text{on } y = g^*, \quad v' = \eta'^{+}_t + U\eta^{+}_X \quad \text{on } y = h^*, \tag{3.5}$$
$$v' = u'f^{-}_X \quad \text{on } y = f^-, \quad v' = u'f^{+}_X \quad \text{on } y = f^+. \tag{3.6}$$

We note that, in general u' depends on y (from Eq. 3.2), and hence now define the averaged velocity

$$\bar{u'}^{+} = \frac{1}{h^* - f^+}\int_{f^+}^{h^*} u'^{+}\mathrm{d}y, \tag{3.7}$$

and similarly for u'^m and u'_-. Then, integrating (3.1) over the channel width and applying the boundary conditions (3.5) and (3.6), we obtain:

$$\eta'^{+}_t + U\eta'^{+}_X + (h^* - f^+)\bar{u'}_X = 0, \tag{3.8}$$

(where we recall that $h^* - f^+$ is constant).

3.1 Case of uniform U

In general, the y-dependence of (3.2) makes further simplifications difficult, but in the case $U_y = 0$ we find that $u' = \bar{u'}$. We then find, using (3.3), that:

$$u'^{+}_t + U^+u'^{+}_X + \frac{1}{k}\eta'^{+}_X = 0. \tag{3.9}$$

We now take a linear combination: (3.8) $+\lambda^+$ (3.9) to obtain:

$$\frac{\partial}{\partial t}\left[\eta'^{+}+\lambda^{+}u'^{+}\right]+\left(\frac{kU^{+}+\lambda^{+}}{k}\right)\frac{\partial}{\partial x}\left[\eta'^{+}+\frac{kU^{+}}{kU^{+}+\lambda^{+}}\left(\frac{(h^{*}-f^{+})}{U}+\lambda^{+}\right)u'^{+}\right]=0. \tag{3.10}$$

In order that the square-bracketed quantities are equivalent, we require:

$$\lambda^{+}=\frac{kU^{+}}{kU^{+}+\lambda^{+}}\left(\frac{(h^{*}-f^{+})}{U^{+}}+\lambda^{+}\right)\quad\Rightarrow\quad\lambda^{+}=\pm\sqrt{k(h^{*}-f^{+})}. \tag{3.11}$$

This implies that $\eta'^{+}\pm|\lambda^{+}|u'^{+}$ is a function of $X-c_{\pm}^{+}t$, where

$$c_{\pm}^{+}=U^{+}\pm\sqrt{\frac{(h^{*}-f^{+})}{k}}. \tag{3.12}$$

Hence we deduce that the solutions take the form

$$\eta'^{+}=F(x-c_{+}^{+}t)+G(x-c_{-}^{+}t), \tag{3.13}$$

$$u'^{+}=\frac{1}{2\lambda^{+}}\left(F(x-c_{+}^{+}t)-G(x-c_{-}^{+}t)\right), \tag{3.14}$$

where henceforth we use the symbols λ^+ etc. to refer to the positive root, and F and G are determined by the relevant boundary conditions.

For the purposes of illustration, we consider the case of a mother tube of width two, which branches into two identical daughters. We prescribe p'^{m} and u'^{m} to vary sinusoidally in time at some point upstream of the branching (for convenience, we take the point $X=-1$). We assume

$$p'^{m}=\alpha e^{it},\quad u'^{m}=\beta e^{it},\quad\text{at } X=-1, \tag{3.15}$$

where the real part is to be understood. From the above, the solution takes the form

$$\eta'^{m}=A^{m}e^{i\left(t-\frac{X}{c_{+}^{m}}\right)}+B^{m}e^{i\left(t-\frac{X}{c_{-}^{m}}\right)}, \tag{3.16a}$$

$$u'^{m}=\frac{1}{2\lambda^{m}}\left(A^{m}e^{i\left(t-\frac{X}{c_{+}^{m}}\right)}-B^{m}e^{i\left(t-\frac{X}{c_{-}^{m}}\right)}\right), \tag{3.16b}$$

$$\eta'^{+}=A^{+}e^{i\left(t-\frac{X}{c_{+}^{+}}\right)}+B^{+}e^{i\left(t-\frac{X}{c_{-}^{+}}\right)}, \tag{3.17a}$$

$$u'^{+}=\frac{1}{2\lambda^{+}}\left(A^{+}e^{i\left(t-\frac{X}{c_{+}^{+}}\right)}-B^{+}e^{i\left(t-\frac{X}{c_{-}^{+}}\right)}\right), \tag{3.17b}$$

Note that (3.17) will also apply in the lower daughter. The amplitudes are determined by applying the boundary conditions, together with continuity of mass and momentum flux. We find:

$$A^{m}=\frac{1}{2}\left(\alpha+2\lambda^{m}\beta\right)e^{-\frac{i}{c_{+}^{m}}},\quad B^{m}=\frac{1}{2}\left(\alpha+2\lambda^{m}\beta\right)e^{-\frac{i}{c_{-}^{m}}}, \tag{3.18}$$

$$A^{+}=A^{m}+B^{m}+(A^{m}-B^{m})\left(\frac{U^{m}(h^{*}-f^{+})-U^{+}}{2\lambda^{m}(h^{*}-f^{+})}\right), \tag{3.19}$$

$$B^{+}=A^{m}+B^{m}+(A^{m}-B^{m})\left(\frac{U^{m}(h^{*}-f^{+})-2\lambda^{+}-U^{+}}{2\lambda^{m}(h^{*}-f^{+})}\right). \tag{3.20}$$

We note the above wave behaviour is very similar to the classical results quoted in e.g. [7,25]; indeed, in the limit $U=0$, we recover the wave equation from (3.8–3.9). However, the solutions for each such vessel in the current branching-flow setting interact via pressures or velocity jumps at the branching junctions. The long-scale interaction problem is self-contained overall once those jumps are prescribed and in fact they are (or would seem to be) given by quasi-steady relations as in earlier work. Nevertheless, we examine the flow–structure interaction within a shorter scale in the following section.

4 The flow close to the branching for small Strouhal number

Now we consider the flow on $O(1)$ lengthscales both for the sake of completeness and for its intrinsic interest. We find this regime is broadly equivalent to that described in [2], and at leading order, the flow is steady. The dependent variables are expanded as follows:

$$p = p_0 + \mathcal{S}p_1 + \cdots, \quad u = u_0 + \mathcal{S}u_1 + \cdots, \quad v = v_0 + \mathcal{S}v_1 + \cdots, \quad \text{etc.}$$

We now introduce a stream function ψ_0 for the leading-order velocities $u_0 = \psi_{0y}$ and $v_0 = -\psi_{0}x$. It is then straightforward to show from leading-order versions of (2.8) that vorticity is constant along streamlines in this region, and hence we obtain the same governing equation as Smith and Jones [2]

$$\nabla^2\psi_0 = -\Omega(\psi_0), \tag{4.1}$$

(where $\Omega(\psi_0) = \omega(x, y)$ is the leading-order vorticity). We can then use Bernoulli's equation to relate the pressure p_0 to ψ_0 via

$$p_0 + \frac{1}{2}(u_0^2 + v_0^2) = H(\psi_0), \tag{4.2}$$

where $H'(\psi_0) = -\Omega(\psi_0)$. Note that the above equations apply in the mother and both daughters, so for the sake of avoiding repetition, the superscripts have been omitted.

On neglecting wall inertia, the pressure is then related to the displacements of the walls by

$$\frac{p_0}{\sqrt{1+h_{0x}^2}} = \frac{1}{k}\eta^+ \quad \text{on } y = h_0, \qquad \frac{p_0}{\sqrt{1+g_{0x}^2}} = -\frac{1}{k}\eta^- \quad \text{on } y = g_0. \tag{4.3}$$

The kinematic boundary conditions on the channel walls give

$$v_0 = u_0 g_{0x} \quad \text{on } y = g_0, \quad v_0 = u_0 h_{0x} \quad \text{on } y = h_0, \tag{4.4}$$

$$v_0 = u_0 f_x^- \quad \text{on } y = f^-, \quad v_0 = u_0 f_x^+ \quad \text{on } y = f^+. \tag{4.5}$$

Far upstream of the branching, without loss of generality, we take the pressure to be zero. Generally, we also set pressure boundary conditions in the daughters. Downstream, the pressure is set to be P_∞^+ in the upper channel and P_∞^- in the lower channel; this is equivalent to prescribing the wall displacements. The boundary conditions are thus

$$p_0^m \to 0 \text{ as } x \to -\infty, \quad p_0^+ \to P_\infty^+ \text{ as } x \to \infty, \quad p_0^- \to P_\infty^- \text{ as } x \to \infty. \tag{4.6}$$

For the sake of subsequent convenience, we denote the velocities far up- and downstream of the branching as follows

$$u_0^m \to U^m \text{ as } x \to -\infty, \quad u_0^+ \to U^+ \text{ as } x \to \infty, \quad u_0^- \to U^- \text{ as } x \to \infty. \tag{4.7}$$

When pressure boundary conditions are specified, these quantities are unknown *a priori* and must be determined as part of the solution. In the simplest case, in which the leading-order flow is uniform far up- and downstream of the branching point, conservation of mass, together with the Bernoulli equation yield:

$$(h^*(-\infty) - g^*(-\infty))U^m = (h(\infty) - f^+(\infty))U^+ + (f^-(\infty) - g(\infty))U^-, \tag{4.8}$$

$$\frac{1}{2}U^{m2} = P_\infty^+ + \frac{1}{2}U^{+2} = P_\infty^- + \frac{1}{2}U^{-2}. \tag{4.9}$$

Elimination between these three equations then yields the unknowns U^m, U^+ and U^- in terms of the known pressures. Strictly, however, for this approach to be valid, we need to be sure that there is no choking of the flow in the intermediate region. Hence we need, at least, to calculate the free-surface positions; we pursue this aim in the following section. Matching to the long lengthscale solution requires $u_0 \to U$, $p_0 \to P$, $v_0 \to 0$ as $x \to \pm\infty$, whilst the higher-order terms obey $u_1 \to u'$, $p_1 \to p'$, $v_1 \to 0$ and $v_2 \to v'$ as $x \to \pm\infty$. We next turn to a specific example.

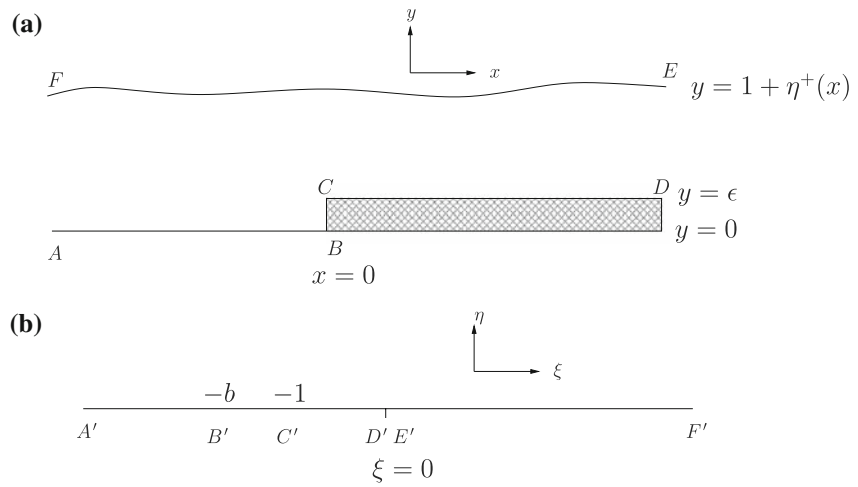

Fig. 2 A symmetric bifurcation with step-like divider in the physical and corresponding transformed planes. **a** Physical plane; **b** Transformed plane

4.1 Irrotational flow over a step-like divider

For simplicity, we now assume that the bifurcation of the channel is symmetric about $y = 0$, so we need only consider the upper half of the channel-divider combination. The symmetry condition implies that, for $x < 0$, $v = 0$ along $y = 0$ (hence the condition is equivalent to assuming an impermeable rigid wall along $y = 0$ for $x < 0$). We set $f^+ = \epsilon H(x)$ (where H is the Heaviside function), so the divider is a simple rectangular step of height ϵ. In the absence of pressure variations, we take the channel wall to be parallel to the x-axis, so $h^* = 1$. We further assume the flow is irrotational at leading order, and hence the streamfunction ψ_0 obeys Laplace's equation. The problem then reduces to finding a complex analytic function $\omega_0(z) = \phi_0 + \mathrm{i}\psi_0$ (where ϕ_0 is the leading order velocity potential) which obeys the boundary conditions. We reiterate that, in this case, the positions of the compliant walls at $y = g$ and $y = h$ are not known a priori. However, since these boundaries are also streamlines, the Bernoulli relation applies on them.

We adopt the approach expounded in a series of papers by King and Bloor [26–28]. In outline, this involves introducing a generalised Schwarz–Christoffel mapping of the physical flow region in the $z(= x + \mathrm{i}y)$ plane to the upper half of the $\zeta(= \xi + \mathrm{i}\eta)$ plane (which we shall term the transformed plane). The mapping is given by an integro–differential equation in terms of a function $\theta(\zeta)$ which specifies the angle of elevation of the free surface at a point z which corresponds to $\zeta = \xi + \mathrm{i}0$ (this function is obviously unknown a *priori*). In the transformed plane, the complex potential $w(\zeta) = \omega(\zeta(z))$ is simple to determine. The procedure is then to substitute this solution for the velocity in the derivative (with respect to ζ) of the Bernoulli equation. This then yields an integro–differential equation for the unknown free-surface elevation function θ. For small free-surface elevations, helpful analytical progress is possible, but the general case is much more difficult.

For the simple geometry described above, the problem is similar to that considered in [27], particularly in terms of the conformal mapping used. However, there are differences in the form of the Bernoulli equation, which lead to interesting new features. For completeness, we briefly describe the details of the solution method below.

The z-plane is mapped to the ζ-plane as shown in Fig. 2, using the transformation

$$\frac{\mathrm{d}z}{\mathrm{d}\zeta} = \frac{-1}{\pi\zeta}\frac{(\zeta+1)^{\frac{1}{2}}}{(\zeta+b)^{\frac{1}{2}}}\exp\left(\int_0^\infty \frac{-\theta(t)}{\pi(\zeta-t)}\mathrm{d}t\right), \tag{4.10}$$

where b is a constant such that $(-b, 0)$ is the image of the origin in the z-plane. The derivation of the form of this generalised Schwarz–Christoffel mapping is given in [28]. Note that when ζ is real and positive, the integral

in (4.10) becomes a Cauchy principal value together with a contribution $\mathrm{i}\theta(\xi)$ that ensures $\mathrm{d}z/\mathrm{d}\zeta$ is an analytic function of ζ. This mapping shifts the points A–F in the z-plane to their counterparts A'–F' in the ζ-plane, as shown in Fig. 2.

The Bernoulli relation on the free surface gives

$$\frac{1}{2}|\nabla\psi_0|^2 + p = \frac{1}{2}U^{m2} = \text{const.} \tag{4.11}$$

Substituting for p from the wall law gives

$$\frac{1}{2}|\nabla\psi_0|^2 + \frac{1}{k}\eta^+\sqrt{1+(\eta_x^+)^2} = \text{const.} \tag{4.12}$$

The flow in the ζ-plane is simply that due to a sink at the origin. Since the incoming flux at $x = -\infty$ is $Q = U^m$, by conservation of mass, the strength of the sink is U^m/π, and the complex potential is hence

$$w(\zeta) = -\frac{U^m}{\pi}\log(\zeta). \tag{4.13}$$

Note that this fact makes it convenient to prescribe the flux into the branching (i.e., set $U^m = 1$), instead of prescribing the pressure P_∞^+, and determining U^m from (4.8) and (4.9). However, these two conditions are not equivalent, as setting the pressure also imposes a condition on the wall displacement, which setting the flux does not.

We now introduce, for subsequent notational convenience, the following:

$$P = -\frac{1}{\pi}\mathcal{P}\left(\int_0^\infty \frac{\theta(t)}{\xi - t}\mathrm{d}t\right) \tag{4.14}$$

where $\mathcal{P}$ denotes the Cauchy principal value. Thus on the free surface $\xi > 0$, the map (4.10) becomes:

$$\frac{\mathrm{d}z}{\mathrm{d}\xi} = \frac{-1}{\pi\xi}\frac{(\xi+1)^{\frac{1}{2}}}{(\xi+b)^{\frac{1}{2}}}\exp\left(P + \mathrm{i}\theta(\xi)\right). \tag{4.15}$$

In order to determine the value of b, we integrate over the image of the step in the transformed plane, to obtain

$$\epsilon = -\frac{1}{\pi}\int_{-b}^{-1}\frac{1}{\xi}\left|\frac{(\xi+1)}{(\xi+b)}\right|^{\frac{1}{2}}\exp P\,\mathrm{d}\xi. \tag{4.16}$$

We now wish to use the Bernoulli relation given above to obtain an equation for the unknown free surface elevation. We begin by noting that the flow velocities on the free surface obey

$$u - \mathrm{i}v = \frac{\mathrm{d}w}{\mathrm{d}z} = \frac{U^m(\xi+b)^{\frac{1}{2}}}{(\xi+1)^{\frac{1}{2}}}\exp(-P - \mathrm{i}\theta). \tag{4.17}$$

For convenience, we now introduce the change of variable $\phi = -(1/\pi)\log\xi$. Upon taking the derivative of (4.12) with respect to ϕ, substituting for the modulus of the velocity from (4.17) and using (4.15), we obtain

$$\mathcal{K}\left(\frac{\pi(b-1)\mathrm{e}^{-\pi\phi}}{(\mathrm{e}^{-\pi\phi}+1)^2} - 2\frac{(\mathrm{e}^{-\pi\phi}+b)}{(\mathrm{e}^{-\pi\phi}+1)}\frac{\mathrm{d}P}{\mathrm{d}\phi}\right) + 2\left(\frac{(\mathrm{e}^{-\pi\phi}+1)}{(\mathrm{e}^{-\pi\phi}+b)}\right)^{\frac{1}{2}}\exp(3P)\tan\theta - \frac{2\eta_0^+\sec\theta\tan\theta\exp(2P)}{\pi\mathrm{e}^{-\pi\phi}}\frac{\mathrm{d}\theta}{\mathrm{d}\phi} = 0, \tag{4.18}$$

where

$$\mathcal{K} = kU^{m2}, \quad P = -\int_{-\infty}^{\infty}\frac{\theta(\mathrm{e}^{-\pi t})}{\mathrm{e}^{\pi(t-r)}-1}\mathrm{d}t.$$

We note from (4.18) that $\mathcal{K}$ in our system plays the same role as $\mathcal{F}^2$ (where $\mathcal{F}$ is the Froude number) for free surface flow under gravity [27]. Equations 4.16–4.18 thus form a coupled system which determines the free surface and the unknown image of the origin, b.

4.2 Case of a thin divider ($\mathcal{S} \ll \epsilon \ll 1$)

We now consider the case of a thin divider ($\epsilon \ll 1$), in which some analytical progress can be made. For consistency with the scalings already introduced, we require $\mathcal{S} \ll \epsilon \ll 1$. Points B' and C' in Fig. 2 will then be close together in the transformed plane. We write $b = 1 + \delta$ with $\delta \ll 1$ (subsequently, we will relate ϵ and δ using (4.16)), and take $\theta = \delta\theta_1 + O(\delta^2)$, $P = \delta P_1 + O(\delta^2)$. Assuming $\phi \sim O(1)$, we find that (4.18) then yields, at leading order

$$\frac{\mathrm{d}P_1}{\mathrm{d}\phi} - \frac{1}{\mathcal{K}}\theta_1 = \frac{\pi \mathrm{e}^{-\pi\phi}}{2(\mathrm{e}^{-\pi\phi}+1)^2}. \tag{4.19}$$

Upon observing that P is a convolution of θ, the above can be solved using Fourier transforms, and the solution was given in [27] as

$$\theta_1 = \frac{\mathcal{K}}{4\pi}\int_{-\infty}^{\infty} \frac{\tau \mathrm{e}^{-\mathrm{i}\phi\tau}}{(\mathcal{K}\tau - \tanh\tau)\cosh\tau}\mathrm{d}\tau + (A\cos(\tau_0\phi) + B\sin(\tau_0\phi))H(1-\mathcal{K}), \tag{4.20}$$

where A and B are constants to be determined, and τ_0 is the positive root of $\mathcal{K}\tau = \tanh\tau$.

For the case where $\mathcal{K} > 1$, the solution can be written

$$\theta_1(\phi) = \frac{1}{2}\mathcal{K}\sum_{n=1}^{\infty} \frac{\beta_n \mathrm{e}^{-\beta_n|\phi|}}{\cos\beta_n(\sec^2\beta_n - \mathcal{K})}, \tag{4.21}$$

where β_n are the positive roots of $\mathcal{K}\beta = \tan\beta$, and we have imposed $\theta_1 \to 0$ as $\phi \to -\infty$. This solution applies irrespective of whether U^m is prescribed, or determined from the prescribed pressures using (4.8–4.9). We note the solution also gives $\theta_1 \to 0$ as $\phi \to \infty$.

The solution for $\mathcal{K} < 1$, with $\theta_1 \to 0$ as $\phi \to -\infty$ imposed is found to be [27]

$$\theta_1(\phi) = \frac{1}{2}\mathcal{K}\sum_{n=1}^{\infty} \frac{\beta_n \mathrm{e}^{-\beta_n|\phi|}}{\cos\beta_n(\sec^2\beta_n - \mathcal{K})} + \frac{\mathcal{K}\tau_0}{2}\left(\frac{\sin\tau_0|\phi| + \sin\tau_0\phi}{2\cosh\tau_0(\mathrm{sech}^2\tau_0 - \mathcal{K})}\right). \tag{4.22}$$

We note the solution (4.22) has a sinusoidal variation in the free-surface elevation (and hence pressure) far downstream, unlike the $\mathcal{K} > 1$ case. Thus the wall stiffness can have a marked effect on the qualitative flow behaviour, at first sight anyway.

However, we note that the final term in (4.18) becomes significant on longer lengthscales. Specifically, we see that if we rescale lengths such that

$$\phi = -\frac{3}{\pi}\log\delta + \hat{\phi}, \tag{4.23}$$

(with $\hat{\phi} \sim O(1)$), then the final term will dominate, and we obtain the solution $\theta_1 = 0$ on this lengthscale upon imposing $\theta_1 \to 0$ and $\hat{\phi} \to \infty$. This allows us to satisfy the downstream boundary condition on the wall (i.e., that θ_1 should tend to zero) for the $\mathcal{K} < 1$ case. It appears to be almost good fortune that in the case $\mathcal{K} > 1$ the solution on the $O(1)$ lengthscale satisfies this condition.

We note that there is an interesting intermediate region where $\phi = -(2/\pi)\log\delta + \phi^*$, in which it appears that there is a balance between all the terms of (4.18). Unfortunatley, however, we have been unable to make any analytical progress in determining the solution in this region.

As in [27], we can now integrate the linearised versions of (4.16–4.18), which give $\epsilon = \delta/2$ and:

$$x(\phi) = \phi + O(\epsilon^2), \tag{4.24a}$$

$$y(\phi) = 1 + 2\epsilon\int_{s=-\infty}^{\phi} \theta_1(s)\mathrm{d}s + O(\epsilon^2). \tag{4.24b}$$

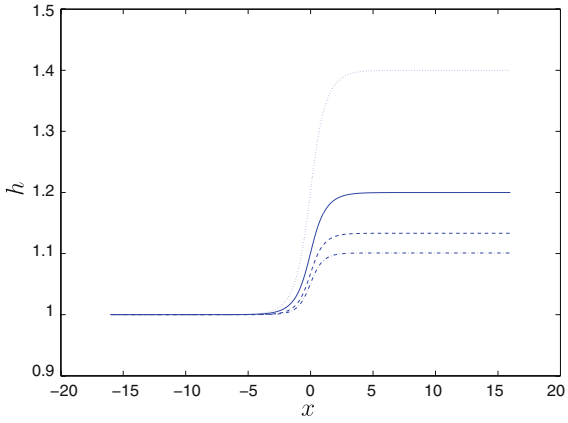

Fig. 3 Flow over a thin step-like divider yielding downstream saturation. $\epsilon = 0.1$ with $\mathcal{K} = 2$ (*solid*), 4 (*dash*), 100 (*dash-dot*) and $\epsilon = 0.2$, $\mathcal{K} = 2$ (*dot*). The divider is given by $f^+ = \epsilon H(x)$

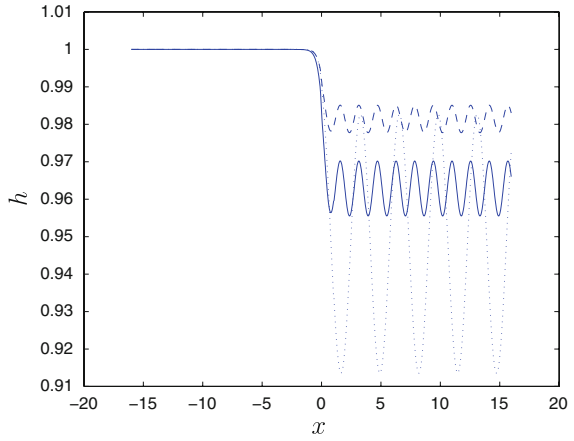

Fig. 4 Flow over a thin step-like divider yielding downstream oscillations (over this short lengthscale) which we conjecture are damped out further downstream: see discussion following Eq. 4.22. Here $f^+ = \epsilon H(x)$: $\mathcal{K} = 0.25$, $\epsilon = 0.1$ (*solid*), 0.05 (*dash*), and $\mathcal{K} = 0.5$, $\epsilon = 0.05$ (*dot*)

The free surface $y = h$ (for $x > 0$) is then given, to $O(\epsilon)$, by

$$h = 1 + \epsilon\mathcal{K}\sum_{n=1}^{\infty} \frac{(2 - \mathrm{e}^{-\beta_n x})}{\cos\,\beta_n(\sec^2\beta_n - \mathcal{K})} \text{for } \theta_1 \text{ given by (4.21)}, \tag{4.25a}$$

$$h = 1 + \epsilon\mathcal{K}\sum_{n=1}^{\infty} \frac{(2 - \mathrm{e}^{-\beta_n x})}{\cos\,\beta_n(\sec^2\beta_n - \mathcal{K})} + 2\epsilon\mathcal{K}\left(\frac{(1 - \cos\,\tau_0 x)}{\cosh\,\tau_0(\mathrm{sech}^2\tau_0 - \mathcal{K})}\right) \text{for } \theta_1 \text{ given by (4.22)}. \tag{4.25b}$$

Plots of these solutions are given in Figs. 3 and 4. For $\mathcal{K} < 1$ (generally reflecting relatively stiffer walls) the mean wall height h is reduced downstream of the branching (indicating the flow is accelerating). By contrast, for $\mathcal{K} > 1$, the flow is decelerated, and hence the channel width must increase.

5 Discussion

We have considered the flow of an inviscid fluid through a branching, compliant-walled channel. This represents a highly simplified model for the flow of blood through an AVM. Since our work is also applicable to non-branching channels with one compliant wall, it may also be of some interest in physiological fluid mechanics more generally, e.g. in situations such as flow through a partially-obstructed vessel. As with other classical analyses of arterial blood flow (see e.g. [7]), or other recent work on collapsible channel flow, we have relied on the assumption that the wall displacements are small in order to make analytical progress. We also assumed a very simple wall model where wall inertia is neglected, and considered only irrotational inviscid flows in symmetric branchings. Although the conformal-mapping technique we used could be extended to asymmetric bifurcations, it can, of course, only be used for irrotational flow. The local problem (Sect. 4) is still to be resolved in full. In particular, it is not clear yet that our assertion that $\theta_1 \to 0$ over a $O(-3/\pi\,\log(\phi))$-lengthscale is strictly justified. Further investigation of this issue, together with numerical simulations for the case of $O(1)$ wall displacements, is evidently needed. However, the overall description of the flow–structure interaction here appears to fit together as required.

Our main result has been to show that the wall compliance can have a very dramatic effect on the behaviour of the flow through the branching. Depending upon the value of the dimensionless parameter $\mathcal{K}$ (which in turn depends upon the wall stiffness) there may or may not be sinusoidal spatial variations in the pressure downstream of the

branching point. However, although the results are interesting, we cannot read too much into them at present, particularly from the clinical viewpoint. Quite simply, the wall model, and assumption of irrotational flow are probably too unrealistic to permit comparison with real AVMs. Extensions to the model, in which some these assumptions are relaxed, together with more experimental data on relevant parameter values, will be needed if we are to be able to make quantitative predictions. As a alternative, it might be useful to consider simplified experimental systems of branching channels, perhaps along similar lines to that described in [29] (which was designed to help gain insight into pulmonary fluid mechanics), where quantitative data is easier to obtain.

The case of many daughters should be discussed here as it is relevant to the AVM application. The conclusion is actually the same in essence as for the two-daughter case studied in Sects. 2–4, in the sense that the responses for each daughter vessel in the multi-branching flow interact (with the mother vessel) via pressures or velocity jumps at the branching junctions. The long-scale interaction problem remains self-contained for the multi-branching configuration as these jumps are determined by the quasi-steady relations of [2], as an analogue of the working for two daughters in Sect. 4 shows. It is interesting that the relations in [2] yield non-unique behaviour and hint at explaining the steal phenomenon mentioned in the introduction but applied now to the more realistic compliant-wall regime. Allowing for viscous effects is feasible, while extending the work further to three-dimensional interactions is desirable (see also [30]) and would add to the realism.

Acknowledgements We would like to thank the referees for their helpful comments. Major support for JEFG was provided by the Engineering and Physical Sciences Research Council (UK) through grant GR/S09418/01. JEFG also acknowledges support from the National Science Foundation (USA), through funding for MBI under agreement no. 0112050.

References

1. Smith FT, Jones MA (2000) One-to-few and one-to-many branching tube flows. J Fluid Mech 423:1–31
2. Smith FT, Jones MA (2003) AVM modelling by multi-branching tube flow: large flow rates and dual solutions. Math Med Biol 20:183–204
3. Smith FT, Ovenden NC, Franke PT, Doorly DJ (2003) What happens to pressure when a flow enters a side branch? J Fluid Mech 479:231–258
4. Smith FT, Purvis R, Dennis SCR, Jones MA, Ovenden NC, Tadjfar M (2003) Fluid flow through various branching tubes. J Eng Math 47:277–298
5. Tadjfar M, Smith FT (2004) Direct simulations and modelling of basic three-dimensional bifurcating tube flows. J Fluid Mech 519:1–32
6. Bowles RI, Dennis SCR, Purvis R, Smith FT (2005) Multi-branching flows from one mother tube to many daughters or to a network. Philos Trans R Soc A 363:1045–1055
7. Pedley TJ (2003) Mathematical modelling of arterial fluid dynamics. J Eng Math 47:419–444
8. Smith FT (1977) Steady motion through a branching tube. Proc R Soc A 355(1681):167–187
9. Blyth MG, Mestel AJ (1999) Steady flow in a dividing pipe. J Fluid Mech 401:339–364
10. Grotberg JB, Jensen OE (2004) Biofluid mechanics in flexible tubes. Annu Rev Fluid Mech 36:121–147
11. Guneratne JC, Pedley TJ (2006) High-Reynolds-number steady flow in a collapsible channel. J Fluid Mech 569:151–184
12. Jensen OE, Heil M (2003) High-frequency self-excited oscillations in a collapsible-channel flow. J Fluid Mech 481:235–268
13. Pedley TJ, Luo XY (1998) Modelling flow and oscillations in collapsible tubes. Theor Comput Fluid Dyn 10:277–294
14. Davies C, Carpenter PW (1997) Instabilities in a plane channel flow between compliant walls. J Fluid Mech 352:205–243
15. Gajjar JSB, Sibanda P (1996) The hydrodynamic stability of channel flow with compliant boundaries. Theor Comput Fluid Dyn 8:105–129
16. Heil M, Waters SL (2006) Transverse flows in rapidly oscillating cylindrical shells. J Fluid Mech 547:185–214
17. Larose PG, Grotberg JB (1997) Flutter and long-wave instabilities in compliant channels conveying developing flows. J Fluid Mech 331:37–58
18. Vito RP, Dixon SA (2003) Blood vessel constitutive models 1995–2002. Annu Rev Biomed Eng 5:413–439
19. Gaver DP, Halpern D, Jensen OE, Grotberg JB (1996) The steady motion of a semi-infinite bubble through a flexible-walled channel. J Fluid Mech 319:25–65
20. Jensen OE, Horsburgh MK, Halpern D, Gaver DP (2002) The steady propagation of a bubble in a flexible-walled channel: asymptotic and computational models. Phys Fluids 14(2):443–457
21. Canic S, Tambaca J, Guidoboni G, Mikelic A, Hartley CJ, Rosenstrauch D (2006) Modelling viscoelastic behaviour of arterial walls and their interaction with pulsatile blood flow. SIAM J Appl Math 67(1):164–193

22. Sherwin SJ, Franke V, Piero J, Parker K (2003) One-dimensional modelling of a vascular network in space-time variables. J Eng Math 47:217–250
23. Pott F, Ray CA, Olesen HL, Ide K, Secher NH (1997) Middle cerebral artery blood velocity, arterial diameter and muscle sympathetic nerve activity during post-exercise muscle ischaemia. Acta Physiol Scand 160:43–47
24. Leutin VP, Pystina EA, Yarosh SV (2004) Linear blood flow velocity in arteries of the brain hemispheres in left-handers and right-handers during hypoxia. Hum Physiol 30(3):290–292
25. Berger SA (1993) Flow in large blood vessels. Contemp Math 141:479–518
26. Bloor MIG (1978) Large amplitude surface waves. J Fluid Mech 84(1):167–179
27. King AC, Bloor MIG (1987) Free-surface flow over a step. J Fluid Mech 182:193–208
28. King AC, Bloor MIG (1990) Free-surface flow of a stream obstructed by an arbitrary bed topography. Q J Mech Appl Math 43(1):87–106
29. Baroud CN, Tsikata S, Heil M (2006) The propagation of low-viscosity fingers into fluid-filled branching networks. J Fluid Mech 546:285–294
30. Bowles RI, Ovenden NC, Smith FT (2008) Multi-branching three-dimensional flow with substantial changes in vessel shapes. J Fluid Mech 614:329–354